River Flow 2010 - Dittrich, Koll, Aberle & Geisenhainer (eds) - © 2010 Bundesanstalt für Wasserbau ISBN 978-3-939230-00-7

Eddy educed entrainment

G. Smart, & D. Plew
National Institute of Water & Atmospheric Research, Christchurch, New Zealand

D. Gateuille.
Laboratoire d'étude des Transferts en Hydrologie et Environnement, Grenoble, France

ABSTRACT: Experiments were undertaken in a rectangular, re-circulating flume to produce conditions of incipient gravel entrainment. Flume hydraulic parameters and bed geometry were designed to simulate a gravel bed river. The flume bed gravel sizes were representative of the river's surface armour layer. Finer river gravel was used to embed the overlying gravel. During the experiments a Particle Tracking Velocimetry (PTV) system was used to visualise turbulent flow structure, and absolute and differential pressure sensors were placed in the surface layer of the bed to measure pressure fluctuations and uplift pressures. Bed surface pressures were recorded at the centre of a circular, flat plate so that measured pressures were not influenced by lift or form drag due to the sensor shape. The PTV system and pressure sensors were synchronised so that flow conditions could be visualised at the time of any unusual bed pressure events. The flume results show that advected turbulent pressure fluctuations are of sufficient magnitude to cause entrainment of bed particles. In addition, the measurements indicate that significant uplift events often arise when a low pressure situation immediately follows high pressure conditions at the bed. It is concluded that residual high pressure within the bed enhances the pressure differential between the bottom and top of a bed particle when the subsequent low pressure zone suddenly arrives above the particle. Along with "tornado-type" vortices, such pressure events can create entraining forces on surface particles in a permeable bed.

Keywords: Entrainment, Critical shear stress, Pressure fluctuations, Gravel, PTV

1 INTRODUCTION

1.1 *Justification*

If the physical processes that govern sediment transport are properly understood, better formulae and models can be developed to assess and manage scour, deposition, sediment related hazards and flood conveyance and to help predict the evolution of past and present fluvial morphology.

1.2 *Background*

Measurements in the Waimakariri river, New Zealand river (Smart, 2005 and 2008) have indicated a direct link between pressure fluctuations within the surface layer of a riverbed and the onset of sediment movement. Using a differential pressure sensor buried in the gravel-bed, these experiments gave strong evidence that pressure fluctuations on and within a gravel bed surface can be sufficient to entrain bed particles when dimensionless bed shear stress is around 0.05. Until now it has generally been assumed that lift and drag forces generated by particle shape are the main mechanisms for the onset of sediment motion. The following experiments, under controlled conditions in a flume, were made in an attempt to reproduce the "induction by suction" phenomenon apparently occurring in the river and to gather further insight into particle entrainment mechanisms.

1.3 *Reference frame and notation*

For the flume experiments, a rectangular reference frame coordinate system is used which has x measured horizontally and z measured upwards from the channel bed. Flume flow was from right to left and x increases in this direction. Velocity components in the x, z and transverse directions

are represented by symbols u, w and v respectively. Deviations from mean values of u and w are represented by u' and w'. A complete list of symbols is given at the end of the paper.

2 EXPERIMENTAL SETUP

2.1 *Flume and hydraulics*

The experiments were carried out in a rectangular, re-circulating, laboratory flume at the National Institute for Water & Atmospheric Research, Christchurch, New Zealand. The effective flume length (with a gravel bed) was 4.7 m. The channel width was 0.12 m. The flume had one plexiglass wall and one steel wall. Water depths were around 0.160 m. A width to depth ratio of less than two was used to limit secondary flow circulation effects. All measurements were taken at the centerline of the flume. The flume inlet was via a horizontal perforated plate with 144 holes (4 mm diameter) per square decimeter in the floor of the flume discharging into a 0.8 m x 0.6 m chamber at the head of the flume. A 0.75 m long, streamwise convex, streamlined taper from the inlet chamber reduced the flow width from 0.6 m to 0.12 m. The perforated plate and contracting inlet conditions were designed to destroy any residual turbulent structures upstream of the start of the flume gravel bed.

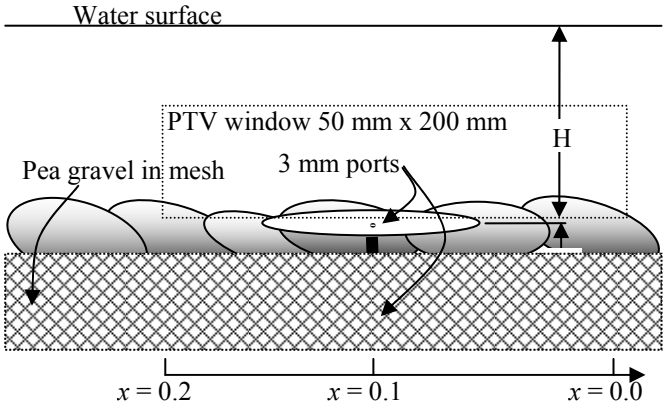

Figure 1. Flume measurement section showing layout and nomenclature. Flow is right to left. Not drawn to scale.

The flume outlet was controlled by adjustable vertical "venetian blind" vanes to set uniform depth conditions through the measurement section of the flume. The flume had a bed slope of 0.018. The coordinate origin of the measurement reference frame was located 100 mm upstream from a bed-plane pressure sensor. Water depth was recorded at three points (at x = -0.23 m, 0.20 m and +0.90 m) by manually measuring the distance from the water surface to the flume reference rail. The location of z = 0 is an arbitrary level, 1.7 mm below the top pressure port. The measuring section is shown diagrammatically in Figure 1.

2.2 *Pressure measurement system*

The laboratory pressure measurement setup was similar to one previously used in the field (Smart, 2008). Figure 2 shows the pressure measurement device when viewed from below. It comprised a 3 mm bed surface port, a 3 mm port buried 61 mm below the bed surface port and a housing containing a differential pressure sensor and an absolute pressure sensor. Absolute pressures were measured at the surface port and differential pressures were measured between the two ports. The bed surface port was situated in the middle of a 50 mm diameter flat circular plate to avoid any local, form-induced pressure variations. The circular plate was installed in the bed plane, slightly below the crest level of the gravel bed surface as shown in Figures 3 and 4.

Figure 2. Under-view of pressure ports. The in-bed pressure port is a 3mm hole in a 6mm copper pipe and the bed-plane sensor port is a 3 mm hole (not visible) at the centre of a 50 mm circular plate. This figure is distorted by perspective.

Figure 3. Typical bed configuration showing sensor plate.

Pressures were measured with Motorola MPX series transducers with ± 0.25% linearity and response time of 1 ms. Pressure head measurement resolution was 0.25mm for the differential transducer (which indicated uplift) and 2.5 mm for the absolute transducer (which indicated water depth). The pressure transducers were located 75 mm away from the sensing ports and connected by rigid copper tubes. Static and uplift pressure measurements were recorded at a frequency of 56.25 Hz over 11 minutes.

2.3 *Gravel bed*

Figure 4. Top view and side view showing the mesh to prevent entrainment of smaller, underlying stones. Note: some surface stones have been removed for clarity.

The bed material was natural river gravel taken from the Waimakariri River, north of Christchurch, New Zealand. The surface gravel was selected to be representative of the surface armor layer of the river and had d_{90} = 66 mm and d_{50} = 57 mm. Finer river gravel with d_{90} = 7.0 mm and d_{50} = 4.6 mm was used under the armor layer to embed surface stones, the housing and the in-bed pressure port. The smaller, sub-bed gravel was enclosed in a flexible 2 mm wire mesh to prevent entrainment of this material into the flow. This is shown in Figure 4. The horizontal permeability coefficient of the *in-situ* bed was 0.064 m/s.

2.4 *PTV eddy tracking*

A high speed movie camera was used to visualize the flow structure by detecting waterborne particles in the flow. Near-neutral-density Pliolite (s = 1.03, passing a 0.5 mm sieve) was used for the tracer particles. Movie recording was carried out in the dark. A vertical light sheet (about 10 mm thick) illuminated only those particles lying above the centerline of the flume.

The digital movie camera was a monochrome Dalsa DS-21-02M30. In order to track particles between subsequent frames at the mean streamwise velocity of about 1.3 m/s, a frame refresh frequency of 164 Hz was used with a resolution of 400 x 100 pixels per frame. Using this resolution, the size of each pixel was approx. 0.5 x 0.5 mm. **P**article **T**racking **V**elocimetry (Nokes, 2009) was used for analysis of movie frames.

In each experiment, the flow above the pressure sensor was filmed for a period of 11 minutes (while bed pressures were also being measured). PTV analysis was then carried out on segments of the captured images at the times of high uplift pressures identified by the pressure measurement system. The PTV analyses were made with the FluidStream 8.0 software from Nokes, University of Canterbury. Images were pre-processed to increase contrast between illuminated particles and the background by subtracting from each pixel the average intensity within a surrounding 5x5 pixel window. Areas of images containing light reflected from the gravel bed were also removed.

Particles were identified in each image based on pixel intensities. Around 400 particles were identified in each frame. Particles were matched to particles in subsequent frames using a combination of a correlation between the location of surrounding particles and predictions based on the velocity of previously matched particles in a window surrounding the particle to be matched. Tracking parameters were optimised by manually tracking about 40 particles. Between 60% - 80% of particles were matched to particles in subsequent image frames. Particle velocities (calculated from the displacement of a particle between frames) were interpolated on to a regular grid 5 mm wide by 2 mm high. Mean velocity components (u, w) were calculated at each grid point. Turbulent fluctuations (u', w') were calculated about these mean values.

2.5 *ADV measurements*

A Sontek micro-ADV was used to measure velocity components at heights ranging from 2.9 mm to 55 mm above the pressure sensor plate for the bed/flow conditions reported herein. ADV measurements of u, v, and w were made at 50 Hz for periods of 160 sec. The ADV probe influenced the flow field and was not used at the same time as PTV measurements.

3 RESULTS & ANALYSIS

Several bed/water depth/slope/flow combinations were measured in the flume to achieve conditions not exceeding the onset of entrainment of surface stones while retaining the ability to track particles between successive movie frames. The results reported here represent the measurements for experimental "bed 6". Five similar PTV and bed pressure experiments (named A-E), lasting 11 minutes each, were run on this bed. Hydraulic parameters for a typical experiment are shown in Table 1 in comparison with measurements made in the Waimakariri River.

Table 1. Hydraulic parameters for Bed 6 run B

Location	Flume Bed 6		Waimakariri R.	
Mean velocity	1.27	m/s	1.48	m/s
Flow*	0.025	m^3/s	1.325	m^2/s
Width*	0.12	m	1.0	m
Depth H**	0.164	m	0.90	m
Water surface slope	0.019	-	0.004	-
d_{50} ***	57	mm	50	mm
shear velocity****	0.175	m/s	0.188	m/s
dim. shear θ	0.034	-	0.045	-
Froude no.	1.0	-	0.5	-
Reynolds no.	0.21×10^6		1.33×10^6	
Grain Reynolds no.	11,550	-	9,400	-

Notes: * unit width assumed for river.
** see Figure 1 for nomenclature.
*** bed surface layer.
**** based on flow depth and slope.

3.1 *ADV measurements*

The vertical profile of streamwise velocity measured with the ADV is shown in Figure 5.

Shear velocity calculated from the log profile fitted to the ADV measurements is similar to the shear velocity based on downslope fluid weight (see Table 1). These ADV streamwise velocity measurements are time averaged but not spatially averaged and the profile extends 54 mm above the 50 mm diameter plate. Consequently, the roughness parameter Zo, based on the velocity profile close the plate, is much smoother than would be found at other locations above the gravel bed.

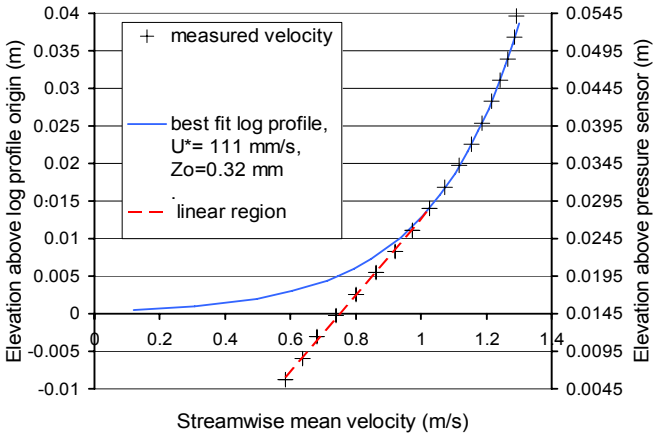

Figure 5. Profile of streamwise velocity above the surface pressure port on Bed 6 (the right to left flow direction is reversed for clarity).

Power Spectral Densities for the component of vertical velocity for a point 10 mm above the circular pressure plate are shown in Figure 6. Velocity components in this case are deviations from the long-term, time-averaged value.

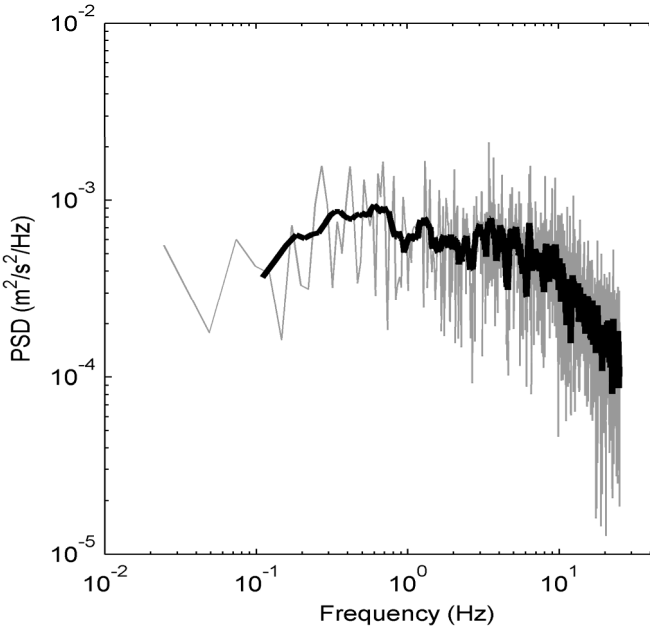

Figure 6. Power Spectral Density (PSD) of the vertical velocity component w' recorded at 10 mm above the circular pressure plate. Raw spectra are shown in gray and a smoothed curve in black.

Power **S**pectral **D**ensity (PSD) decreases above about 10 Hz and below about 0.4 Hz. A sample longer than about 5 s (2@ 0.4 Hz) is necessary to fully capture the largest of the eddy fluctuations and time-scales conventionally assumed relevant to turbulent eddy generation thus range from 0.1 s to 2.5 s. Length scales (based on mean velocity) range from 0.13 m to 3 m.

3.2 *Pressure records*

Fourier analysis of pressure measurements (not shown) indicates fairly flat PSD with a minor increase in energy concentrated around frequencies of 1.58 Hz and 9.5 Hz in both the bed pressure and uplift pressure series. The pressure PSD lines are attenuated much more sharply (than for the velocity PSD) above 0.1 Hz, possibly indicating some mechanical smoothing of higher frequencies in the pressure measurement apparatus.

Two examples of bed pressures, uplift and calculated sub-bed pressures are given in Figure 7 (sub-bed pressure = measured bed pressure + measured uplift). The bed pressure heads have the 61mm static head difference (between the sensor ports) removed for comparison of the fluctuations in the series. At times 14:06:09.1 and 14:06:23.0, significant uplift peaks are shown. These two uplift events were the largest recorded during experiment 6B. Over the full experiment, the recorded pressure time-series have approximately normal distributions of values. Summary statistics for this experiment are given in Table 2.

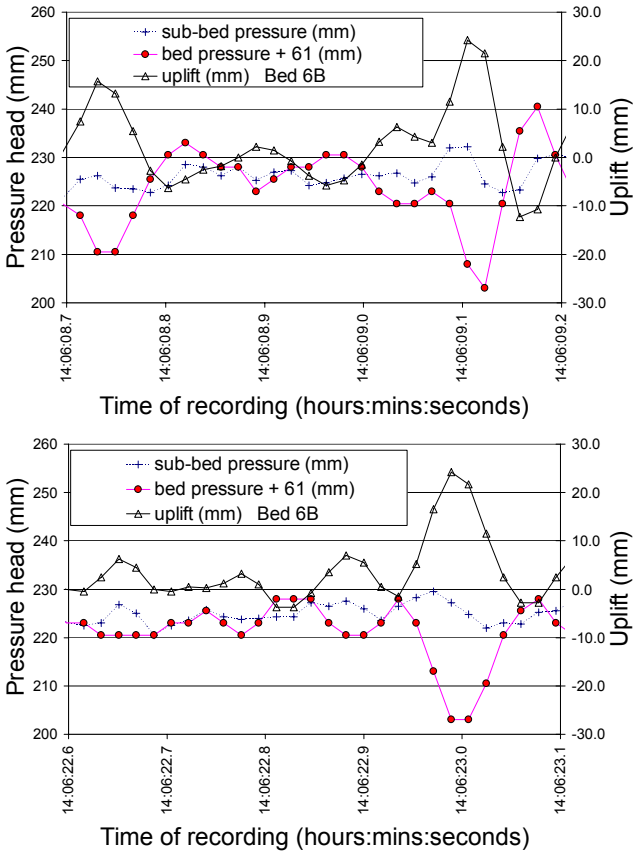

Figure 7. Two half-second excerpts from experiment 6B showing the bed pressure, sub-bed pressure and uplift pressure.

Table 2. Statistics from 8 minutes of pressure measurements recorded at 56.25167 Hz during experiment 6B

	bed pressure		uplift pressure	
Mean value	164.98	mm	-0.28	mm
median value	164.5	mm	-0.25	mm
mode	167	mm	-1.5	mm
minimum value	139.5	mm	-24	mm
maximum value	189.5	mm	24.25	mm
standard deviation	5.65	mm	5.23	mm
skewness	.236	mm	.039	mm
sample size	27000		27000	

A strong inverse relation between bed pressures and uplift pressures is shown in Figure 8 and Figure 7. The linear trend has high uplifts occurring with low bed pressures and vice versa. 81% of the uplift pressure variation can be explained by the bed pressure variation (r = -0.90). There is considerable scatter about the linear trend line on Figure 8 which is partly explained by lagged cross-correlation (r = -0.82 for bed pressure leading uplift by one 18 ms timestep and r = -0.51 for bed pressure lagging uplift by 18 ms). There is a very small (positive) relation between instantaneous values of bed surface pressure and the corresponding sub-bed pressure. Only 15% of sub-bed pressure variation is explained by variation in the bed pressure.

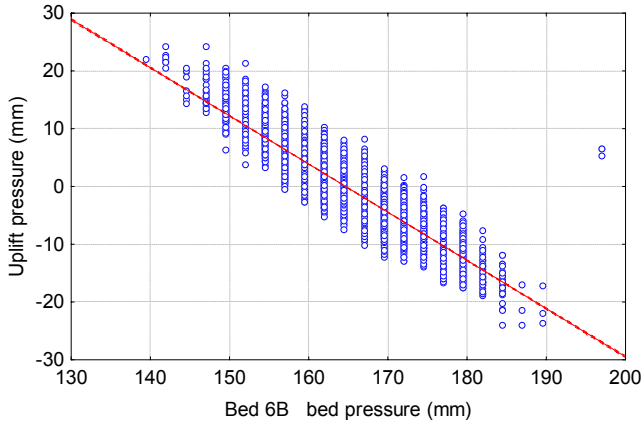

Figure 8. Relation between uplift and bed pressure. The outliers at the far right are unexplained isolated spikes in the bed pressure data.

For conditions of imminent particle entrainment it is the rare and extreme values of uplift, such as those shown in Figure 7, that are of interest. The maximum uplift head for the experiment summarized in Table 2 is equivalent to a pressure difference of 238 Pa which is sufficient to lift stones smaller than 23 mm in diameter. From analysis of all such peaks in the experiments it appears that extreme uplift events typically show sub-bed pressure rising just before a large fall in the on-bed pressure (see Figure 7). The combination of high sub-bed pressure and low on-bed pressure creates a larger uplift pressure. This effect is discussed further in the next section.

3.3 *Image analysis*

The PTV technique used captures 2-dimensional, instantaneous snapshots of the flow and may mis-interpret some 3-dimensional features. An example of actual particle trajectories is shown by a time exposure in Figure 9 where the flow direction is from right to left. Particle "A" is about 50 mm above the bed. In 0.04 s it travels 68 mm from A1 to A2. A calculation based on its start and finish points indicates a horizontal velocity u = 1.68 m/s and a vertical velocity w = –0.2 m/s. PTV should indicate similar velocity components. In the area just above the sensor plate, there is a change in the flow pattern from fast streamwise motion to turbulent, vortical motion. This "vortex swarm" area was swept in from upstream. In this area, during 0.04 s, particle "B" starts about 6 mm above the plate and spirals upwards and downstream to finish at point B2. The first part of particle B's path is dim as it lies at the limits of the 10 mm wide light sheet. The time exposure trajectory indicates that particle "B" rotates 4 times around a vortex axis between B1 and B2. For the last of these cycles, particle B has a tangential velocity of about 0.75 m/s at a radius of about 6 mm. For this tangential velocity, the Bernoulli-predicted pressure drop at the core of the vortex ($\rho\, v_t^2/2$) would be 280 Pa. PTV can not identify these features due to a combination of insufficient resolution, matching complexity and interpolation smoothing.

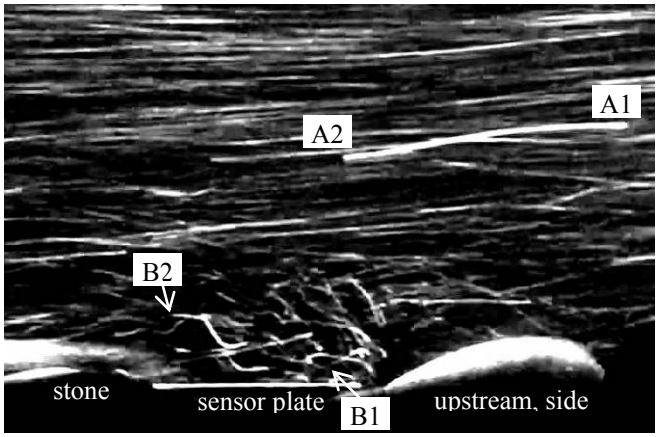

Figure 9. Side view of the flow over the sensor plate during time exposure of 0.04 s. Flow is from right to left. A vortex swarm, generated upstream, is passing over the plate.

A second particle track, very similar to that of particle B, is evident in Figure 9 just below that of particle B. If these two vortices have the same rotational direction they are likely to combine into a single, larger vortex. Neither the time-exposure nor the PTV technique can fully capture such larger vortices if their diameter is greater than the 10 mm thickness of the illuminating light sheet.

Figure 10 shows another time-exposure, similar to that shown in Figure 9, with particles visible on the periphery of a passing "tornado-type" structure. The particle near C is in the light sheet for about one quarter of a spiralling revolution. The 26 mm diameter of this trajectory indicates a vortex tangential velocity of 0.5 m/s and the Bernoulli-predicted pressure drop at the core of the vortex would be 125 Pa.

Figure 11 shows a sequence leading up to the time at which a large uplift pressure was detected by the pressure sensor. Mean flow is from right to left. In contrast with the time exposures, Figure 11 shows deviations from mean velocity (as arrow vectors) and vorticity (as a background grayscale). Darker areas are circulating clockwise and lighter areas are circulating counter-clockwise. Each image gives a cross-sectional view of the flow from 100 mm upstream of the sensor plate port to 80 mm downstream of the port.

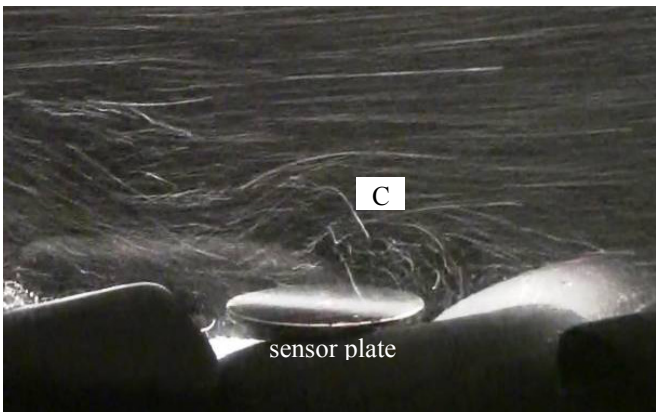

Figure 10. Oblique view during a time-exposure of 0.04 s while a vortex was passing the plate. Flow is right to left.

The images indicate larger circulation patterns but do not reveal spirals or smaller eddy. The images A-D in Figure 11 coincide with the uplift pressure peak shown at 14:06:23 on the lower graph of Figure 7. In image A (at the top), flow downstream of the dotted line is slower than mean downstream flow velocity (vectors point upstream) and flow upstream of the line is faster than average. At point 1 there is a strong clockwise eddy bringing flow into the plane of the cross-section. Flow is towards the bed at the upstream edge of the sensor plate. Image B shows the situation 6 ms later than image A. The slow flow now extends further upstream near the bed and the faster flow extends further downstream 50 mm above the bed. Between these zones the flow is starting to roll up and form an eddy at point 2. Above the plate there is high velocity

towards the bed. Image C shows flow circulation patterns 12 ms later than image B. The line between the zones is stretched further, roll-up eddy 2 has strengthened and moved downstream and eddy 1 has been stretched in the streamwise direction. At the plate and further upstream, velocities are no-longer directed towards the bed. Image D shows flow circulation patterns 12 ms later than image C. The faster flow has swept the slower flow downstream. Eddies 1 and 2 have collided. There are strong velocities moving upwards from the bed.

4 SUMMARY & DISCUSSION

For the bed surface layer of the flume, dimensionless shear stress (Shields θ) was 0.034, somewhat less than the critical value, to ensure that the bed would remain intact during the experiments. During experiment 6B, the maximum uplift pressure head measured was 24.25 mm (238 Pa). Theoretically, this is sufficient to lift a spherical particle 23 mm in diameter and the finer underlying flume gravel could have been entrained if it were not held in place by a restraining mesh.

Maximum uplifts recorded in experiments 6A, 6C, 6D, and 6E were sufficient to exceed the particle weights if applied over gravel spheres with diameters of 25, 34, 34, and 39 mm respectively. Because the pressures occurred above a flat plate, these uplifts show that advected pressure fluctuations alone can be of sufficient magnitude to lift bed particles when conditions are suitable for entrainment as implied by Shields criteria.

The uplift events were rare with only 1 - 3 extreme uplift events found to occur during each 11 minute recording period. On the basis of a normal distribution of uplift values and using the parameters in Table 2, uplifts exceeding 20 mm could be expected to occur 2 times during an 11 minute period (recording at 56.25 values per second). Uplifts larger than 20 mm should be much rarer and it may be that extreme uplifts occur slightly more frequently than indicated by a normal distribution.

Two particle tracks analysed in Section 3.3 implied Bernoulli pressure drops of 280 Pa and 125 Pa at the centre of the eddies. These eddy pressure drops occurred near the bed surface. Figure 8 showed that there is a strong inverse relation between bed surface pressure and uplift pressure. Consequently the particle tracks provide further evidence that advected eddy circulation pressures may be of sufficient magnitude to entrain bed particles during conditions for which entrainment is implied by Shields criteria.

Figures 7 and 11 show that the uplift on embedded particles can be greater than the uplift at the bed surface if the bed is pressurised just before a low pressure event arrives at the bed surface. However, there is an anomaly between Figure 7 and Figure 11. While the sequence of pressure loading and unloading of the bed, shown in Figure 11, takes place over a period of about 30 ms (5 frames at 164 Hz), the corresponding pressure changes in Figure 7 take place over about 53 ms (3 samples at 56.25 Hz). This difference could be caused by attenuation of high frequency pressure measurements as noted in section 3.2.

Another point for discussion is that for several of the recorded extreme uplift pressure events, there was no obvious contributing event observable in the PTV data. This may be due to insufficient trackable particles within the reference frame during the event, pressure fields responding to events outside the 10 mm wide light sheet or to other 3D effects not evident in the 2D PTV visualisation. Nelson *et al* (2001) similarly found that instantaneous lift forces on gravel particles do not correlate well with local instantaneous velocity measurements.

5 CONCLUSIONS

In-bed pressure measurements, vortex rotational velocities and PTV made above a flat plate, indicate that particle entrainment could result from advected pressure fluctuations. The entrainment is induced without lift and drag forces generated by the shape of the lifted particle. Measurements indicate that significant uplift events can occur when a low pressure event immediately follows high pressure conditions at the bed. It is concluded that residual high pressure within the bed enhances the pressure differential between the bottom and top of a bed particle when the subsequent low pressure event arrives above the particle. Along with “tornado-type” vortices, such pressure events appear to create significant lift forces on particles in a permeable bed.

ACKNOWLEDGEMENT

Research was made under contracts CO5X0409 and CO1X0812 from the Foundation for Research, Science and Technology (New Zealand).

REFERENCES

Nelson, J.M., Schmeeckle, M.W. and Shreve, R.L. (2001). Turbulence and particle entrainment. In Gravel Bed Rivers 5, Mosley M.P. (ed.) N.Z. Hydrological Soc., Wellington New Zealand, 221 –240

Nokes, R.I. (2009). Streams Version 1.00 System Theory and Design, Department of Civil and Natural Resources Engineering, University of Canterbury.

Smart, G.M. (2005). A novel gravel entrainment investigation. In River Coastal and Estuarine Morphodynamics 2005, Ed. Parker & Garcia, Balkema, 65-69.

Smart G.M. (2008). Pressure fluctuations and entrainment on a gravel river bed. River Flow 2008, Altinakar, Kokpinar, Aydin, Cokgor & Kirkgoz eds, 817-824.

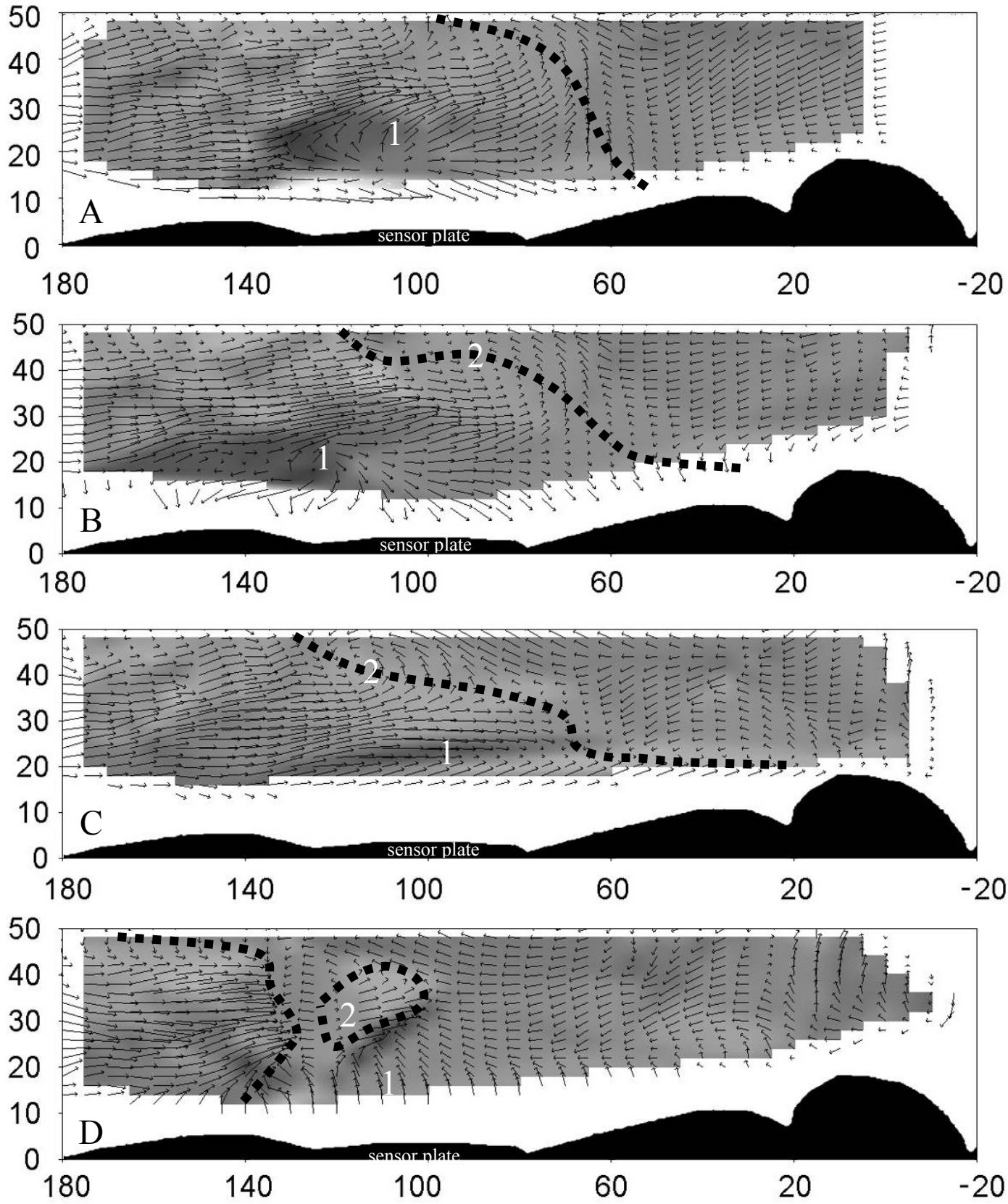

Figure 11. Turbulent velocity vectors (u',v' resultant) 30 ms, 24 ms, 12 ms and 0 ms (respectively from top to bottom) before the peak of a significant uplift event. Flow is right to left. Labeled points are described in Section 3.3.